Use of UAV photogrammetric data in forest genetic trials: measuring tree height, growth, and phenology in Norway spruce (*Picea abies* L. Karst.)

Thomas Mørtvedt Solvin[*], Stefano Puliti and Arne Steffenrem

Norwegian Institute of Bioeconomy Research, Norway

*corresponding author: Thomas Mørtvedt Solvin, thomas.solvin@nibio.no, Norwegian Institute of Bioeconomy Research, P.O. Box 115, Ås NO-1431, Norway

Keywords: UAV, drone, *Picea abies*, growth, phenology, breeding

Abstract

Phenotyping of genetic resources that are used for development of new improved and adapted forest reproductive materials is costly. Therefore, high-throughput-phenotyping from a standard equipped unmanned aerial vehicle (UAV) with a RGB (red, green, blue) camera was used to develop a canopy height model (CHM) of a dense field trial of 15-year-old trees of Norway spruce. The site represents a typical situation of genetic testing on abandoned farm field land, where spacing between trees often are around 1-1.5 m. The CHM was used to estimate total height, intra-annual height growth and phenology of individual trees. The estimates were based on individual tree grid cells assigned according to the original planting grid. Intra-annual growth and phenology could not be estimated accurately, whereas total tree height to the uppermost whorl was accurately estimated provided that the trees were correctly identified. However, the apices of suppressed trees were often misidentified due to overhanging branches from more dominating neighboring trees. The method represents a cost and time efficient alternative to manual height measurements of the intermediate and dominating trees in closed stands. The accuracy is sufficiently high for most breeding purposes when total tree height is the target trait.

Introduction

Different remote sensing techniques are being implemented in forest operations and research. For the purpose of high-throughput-phenotyping individual trees in selected stands, unmanned aerial vehicles (UAV) have promising features as the range of flights are suitable and they can collect high resolution data from cameras or sensors. Hence, UAV data are increasingly used to measure the properties of trees and forests. The UAVs have the ability to rapidly acquire very high resolution 3D and spectral data over entire stands making them an appealing alternative to time-consuming field surveys (Puliti et al. 2019). Previous studies have had promising results for the use of UAV to measure tree height (Ganz et al. 2019; Karpina et al. 2016; Krause et al. 2019; Torres-Sánchez et al. 2015), tree height growth (Dempewolf et al. 2017; Guerra-Hernández et al. 2017), volume (Santini et al. 2019) and phenology (Berra et al. 2019; Park et al. 2019). The studies represent a large variation

with respect to species, type of sensors, traits measured, field conditions, tree identification methods and other parameters which may be important for the results.

Height measurements with UAVs are usually based upon digital surface models (DSM) generated from 3D photogrammetric analysis of overlapping RGB (red, green, blue) images, or more seldom from LiDAR laser scanning. Other than the accuracy of the 3D representation of the trees themselves, two important factors for sound estimates are the precise detection of individual tree crowns and the quality of the digital terrain model (DTM). Often, automated methods must be supplemented by manual methods to ensure the correct detection of tree positions e.g. Ganz et al. (2019), Krause et al. (2019). Phenology assessments have mostly been done for deciduous trees based upon color-related measures, e.g. by Klosterman and Richardson (2017) and Park et al. (2019), but findings also suggest that this can be done with conifers (Berra et al. 2019).

Norway spruce (*Picea abies* L. Karst.) is the most economically important forest tree species in northern Europe and is subject to breeding programs in the Nordic countries, Sweden, Norway and Finland (Haapanen et al. 2015; Jansson et al. 2017). In addition to growth traits such as tree height and diameter, growth phenology is important for optimal deployment with respect to climatic adaptation and growth performance due to the seasonal cycle of growth and dormancy. Measuring height and characterizing phenology manually in breeding trials are laborious and expensive tasks especially as the trees get taller in long-term trials.

In this study we wish to examine the possibility of high-throughput-phenotyping of a densely spaced trial of fifteen-year-old trees of Norway spruce representative of the phenotypic variation found in provenance and genetic trials planted as single-tree-plots. We aim at developing a robust method transferable to other trials of the same species, by means of a simple model where local maxima from a UAV derived canopy height model (CHM) are used as direct measurements of tree height (objective 1). We further test whether intra-annual UAV based measurements of the canopy height are sufficiently accurate to form the basis for growth curves which can describe the vegetative intra-annual phenology of individual trees (objective 2). The last objective (objective 3) was to evaluate the measurement error from using UAV in phenotyping in terms of implications for breeding.

Materials and methods

Plant material and field trial

The material consisted of individuals of Norway spruce produced by somatic embryogenesis under different temperatures, described in Kvaalen and Johnsen (2008). They were propagated as full-sibs from one family, and used for an epigenetic experiment (experiment 3 in Kvaalen and Johnsen (2008)). The genetic information, however, has not been analyzed in this study. The field trial was established at Hogsmark (59.67°N, 10.72°E, 85 m a.s.l.), Norway in May 2007, as single tree-plots with 1 meter spacing between trees, which were then three years of age from germination. There were 67 rows and 15 columns (13 on row 1-39), i.e. 927 trees in total, covering approximately 900 m^2. The mean annual temperature and the mean annual precipitation sum at the trial site for the 1961-1990 reference period were 5.4°C and 920 mm respectively. The trial was established on former agricultural soil with a high clay content.

The trial was used as a case study relevant for genetic trials since we know on beforehand that the variation in growth and phenology between trees is large. The genetic structure of the trial was, however, ignored.

Manual data collection in 2018

Total tree heights accomplished after the growth seasons of 2017 and 2018 were measured on a subset of the trial (241 trees) on November 27, 2018 using a rod marked at each decimeter. The height accomplished in 2017 was measured to the uppermost whorl as these are distinct in Norway spruce. The measured trees were evenly distributed in the trial with the addition of the 90 trees that were studied more in detail and photographed multiple times in 2018 (cf. below). These 90 trees were not evenly distributed in the trial.

Bud flush assessments and leader shoot measurements, both used to describe the intra-annual growth phenology, were based upon photographs of the upper internode taken with a GoPro Hero 5 camera mounted on a telescope rod and placed 74 cm from a white painted background with a measurement scale. The camera was operated from ground with a smartphone. The camera setting "Field of view" (FOV) was set to "linear" (LINR). It was emphasized that the leader should be in contact with the plate when photographed. However, we did not always succeed and some distance between shoot and background plate often occurred. On May 22, 2018 all living trees were photographed, while 90 selected trees were additionally photographed on the following seven dates: June 4, 11, 19, 28, July 5, 23 and November 7 (missing four trees on June 4). Bud flush was scored according to the Krutzsch (1973) scale from the images of the 852 living and not severely damaged trees taken on May 22, 2018.

UAV data collection and processing

Multi-temporal UAV RGB image data were acquired during six flights conducted throughout the 2018 growing season (April 29, May 22, June 9, June 23, July 13, October 18). No apical growth had started at the first date (April 29), and all annual leader growth had ceased at the last date (October 18).

The image data were collected with a DJI Phantom 4-pro (DJI 2016) equipped with a 1-inch 20 MP global shutter RGB imaging sensor. In order to reduce as much as possible inconsistencies due to varying light and atmospheric conditions amongst images obtained at different dates, all flights were conducted at 12:00 during sunny days with wind speed <1 m sec^{-1}. The flight planning and control software DJI ground Station Pro (DJI 2018) was used for the UAV operations. The camera was fixed at a 90° angle to ensure the acquisition of nadir images and automatic settings for shutter-speed, aperture, and ISO were adopted. Furthermore, as means to acquire very precise data, the UAV imagery was acquired at low altitude (approximately 40 m above ground) with high overlap (i.e. 80% forward and 70% lateral overlap), and with perpendicular flight lines. This resulted in a ground sampling distance (i.e. size on the ground of each pixel) of 1 cm. Ten ground control points (GCPs) were measured in the field and marked with permanent wooden pegs. These were then used in the structure from motion optimization to correctly georeference the 3D model processed from the UAV images. For each UAV data acquisition, the same GCPs were used and prior to each flight the markers were cleared from herbaceous vegetation to avoid the misregistration of the multitemporal UAV 3D models in the z axis. An overview of the study area is provided in Figure 1.

Figure 1. Overview of the study area including the locations of the ground control points, height reference points and the single tree grid cells.

The raw UAV images were processed into a high resolution orthomosaic (1 cm) and a 3D digital surface model (DSM; 2 cm) using Agisoft Metashape professional edition (Agisoft 2019). The photogrammetric processing steps and parameters are summarized in Table 1. The parameters were selected to ensure best quality outputs.

Table 1. Processing steps and parameter setting adopted to process the UAV images using Agisoft Metashape professional edition.

Processing order	Parameter settings
Image alignment	• Quality: highest
	• Reference preselection: yes
Optimize alignment	• Fit all values other than b1, b2, p3, p4,
GCP manual placement	
Build dense cloud	• Quality: high
	• Depth filtering: mild
Build DEM	• Source: dense cloud
	• Interpolation: enabled
Data export	

The DSM consists of a detailed 3D representation of the canopy surface where each pixel holds the height above the geoid. A pre-existing digital terrain model (DTM) from airborne laser scanning (ALS) was available for our study area from 2014. The ALS data were available from the publicly available

database in Høydedata.no and further details can be found in the ALS acquisition project report (Blom 2014). The point density was on average 5 points m^{-2} and the ALS data were classified by the data provider into ground and vegetation points according to industry standards (Axelsson 2000). Using the ground points, a 1 m resolution DTM was generated using a triangulated irregular network. The ALS data were in Euref-89, UTM 32 N coordinate system. By subtracting the DTM from the DSM obtained by UAV we obtained a canopy height model (CHM) representing the height of each pixel above ground. The CHM formed the basis of all the following analyses. The unit of the CHM is meter (m).

While DTMs from airborne laser scanning are often considered as truth, in areas that are densely vegetated, such as our trial area, the DTM may be biased. Thus, to account for potential sources of error in this DTM, we measured the ground height of 49 height reference points using a centimeter accuracy Topcon GR5 global navigation satellite system receiver (Topcon 2018) fitted with cellular communication for real time kinematic correction live via the Global System for Mobile communication network. The location of the points was selected opportunistically by walking through the stand in a systematic fashion (i.e. strips) and by performing measurement where GPS signal was strong enough to ensure a centimeter accuracy. Both the walking and the measurements were influenced by the density of the vegetation resulting in most of the ground control heights being placed in canopy openings. However, in some areas the canopy was too dense to allow receiving any GPS signal. We estimated the bias as the average difference among the measured elevation and the airborne laser scanned model elevation for all the measured points.

Statistical methods

The CHM provides a raster layer for each day of UAV measurement with approximately 2 cm x 2 cm spatial resolution. The original planting grid (1 m x 1 m) was digitized and used to tessellate the study area so that each tree corresponded to a grid cell. This approach was adopted rather than an automated single tree detection method in order to reduce the uncertainties due to detection errors. Furthermore, it is often the case for such genetic trials that a map of the original planting grid is available. Measures of tree height, tree growth or tree phenology were based upon variables derived from the CHM within each grid cell. These variables included the maximum value of the CHM (CHMmx) and the highest estimated point within a 20 cm radius from the grid cell center (CHMmx20). The latter was included as CHMmx in some cases corresponded to branches of taller neighboring trees, thus in CHMmx20 we tried to exclude tall peripheral pixels. The variables from the different dates of measurement are hereby referred as CHMmx_1, CHMmx_2…CHMmx_6, where the number indicates the chronological order of the UAV data acquisition from April 29. Furthermore, to model growth we also included the difference between CHMmx_6 and CHMmx_1 (ΔCHMmx) and between CHMmx20_6 and CHMmx20_1 (ΔCHMmx20) as direct measure of the annual growth. All analyses were done in R (R Core Team 2017).

Tree height and total annual height growth

Total tree height accomplished after the growth season in 2017 was estimated from the UAV variables as CHMmx_1 and CHMmx20_1. The values were validated against the manual measurements with measurement rod which we assumed to be the true value (H17). For height increment in 2018 the values of ΔCHMmx and ΔCHMmx20 were also validated against the manual measurements with measurement rod. We provide error estimates of the same types as (Krause et

al. 2019), see also Larjavaara and Muller-Landau (2013), separating total error (RMSE) from systematic (ME) and random error (SDE) as follows:

RMSE (root mean squared error) = $\sqrt{\frac{1}{N}\sum_{i=1}^{N}(x_i - y_i)^2}$ (1)

ME (mean error) = $\frac{1}{N}\sum_{i=1}^{N}(x_i - y_i)$ (2)

SDE (sample standard deviation of error) = $\sqrt{\frac{1}{N-1}\sum_{i=1}^{N}(x_i - y_i - ME)^2}$ (3)

Here the variable x_i is the phenotypic value of individual i predicted from the CHM, y_i is the manual measurement of individual i used for validation and N is the sample size. We also calculated the Pearson's (product moment) correlation coefficient (r) between x and y with p-value from a two-tailed t-test and the Pearson's correlation coefficient between the differences x - y and y to look for dependencies between the errors (x - y) and the actual trait value (y).

We observed that the ME of the UAV variables for total tree height obtained before onset of growth in 2018 corresponded approximately to the length of one year's increment. Since the basal area of an apical bud is relatively small compared with the resolution of the CHM, we hypothesized that the maximum height observed in the UAV data is not the height of the apex, but the upper-most whorl due to the vertical smoothing of the 3D surface typical of photogrammetric data. If, so the UAV variables from the last flight date in 2018, when the height growth had ceased and a new whorl had formed, should approximate the height accomplished after the 2017 season; although this might depend on the architecture of the whorl (e.g. how the sidebranches are angled, or if there are double leaders). We therefore also used the variables CHMmx_6 and CHMmx20_6 to estimate H17.

Phenology

To estimate phenology variables, growth curves were estimated for individual trees' CHMmx by means of the UAV variables from the different flight dates fitted to a three parameter Weibull function:

$$w = 1 - e^{-(\frac{t-a}{b})^c}$$ (4)

, where $w = \frac{z - z_{start}}{z_{end} - z_{start}}$, where z is the UAV variable value at day t (within the active growing period). The values z_{start} and z_{end} are the values of the UAV variable at the first and last day of measurement respectively, i.e. before and after the active growing period. The variable t represents the number of days after March 31. The model was fitted as a non-linear regression with the R-function *nls* with algorithm="port" and starting values a=50 (1, 52), b=10 (1, 100), c=1 (1, 5) (lower and upper parameter bounds in parenthesis).

As a proxy for phenology characterized by growth initiation and cessation, the date of 5 % and 95 % completed growth (Day05 and Day95, respectively) were calculated for each tree as the value of t giving w = 0.05 and w = 0.95 respectively.

Pearson's correlation coefficient was calculated between Day05 and Day95, and the manually scored bud flush (Krutzsch) value. Krutzsch values were transformed to normal score by Blom (1958)'s method before correlations were calculated. The hypothesis was that Day05 represents the growth initiation and should correlate (negatively) with bud flush (Krutzsch score).

Out of the 90 trees where we had manual measurements of leader elongation, 66 were possible to fit to a growth curve for CHMmx at the six dates. Out of these trees 20 were selected for a more detailed study to see if it was possible to use UAV data to create growth curves for individual trees. The actual length of the leaders at each date was measured directly on the images from the GoPro camera using the ImageJ software (v1.51j8) (Rasband 1997-2008) by drawing a segmented line that followed the shoot. As we were often not able to place the shoot completely in contact with the plate, we estimated the distance from the shoot to the plate by visual inspection and performed a correction by multiplying the measured length with the distance between the shoot and the camera and dividing by the distance between the plate and the camera. To these measurements we fitted the Weibull growth curve. We did not repeat this process for all the 66 trees because the CHMmax soon proved to be a poor estimator of the very apex of trees, making the growth curves inaccurate. Instead we used the 20 selected trees to study examples illustrating the issues of using UAV data collection. Comparisons of growth curves based upon UAV measurements and manually taken photographs for three trees can be seen in Figure 5. UAV photos and CHM can be seen in Figure 4.

Implications for breeding

To evaluate the implications of the measurement accuracies for genetic trials and breeding, we considered how the measurement error in selection for breeding would affect the expected response to selection. If selection is implemented as allowing a proportion p of individuals with highest trait value to reproduce, i.e. individual truncation selection, the predicted response (R_{ind}) can be given by the following version of the breeder's equation:

$$R_{ind} = i\sigma_A h \tag{5}$$

, where i is the selection intensity, that is the difference in mean phenotypic value between selected individuals and all individuals (population mean) in units of σ_P, which is the population phenotypic standard deviation, σ_A is the standard deviation of breeding values (additive genetic standard deviation) and $h = \sqrt{h^2}$ is the square root of the heritability. The heritability is equal to the variance of breeding values as a fraction of the phenotypic variance and is given by:

$$h^2 = \frac{V_A}{V_P} \tag{6}$$

, where $V_A = \sigma_A^2$ is the additive genetic variance and $V_P = \sigma_P^2$ is the phenotypic variance. The selection intensity i can be derived from p (Falconer & Mackay 1996). In a mixed model analysis of a genetic trial the random measurement error would manifest itself as part of the residual variance component which is included in the phenotypic variance used in the denominator of the heritability calculation. A systematic measurement error (defined here as ME) on the other hand would not affect variance components and therefore not heritability estimates. Under the assumption that the random measurement error is independent of the actual trait value, the estimated reduced heritability due to measurement error is:

$$h^2_{reduced} = \frac{V_A}{V_P + SDE^2} = \lambda h^2 \tag{7}$$

, where SDE^2 is the estimated variance of measurement error and is the squared value of SDE from equation 3 and λ is a reduction factor of heritability due to measurement error and is given by:

$$\lambda = \frac{V_P}{V_P + SDE^2} \tag{8}$$

(Ponzi et al. 2018, and references therein). We can consider the quantity $V_P + SDE^2$ an observed phenotypic variance. Because selection is based upon the measured values, the selection intensity i is in units of the observed phenotypic standard deviation ($\sqrt{V_P + SDE^2}$) and the reduced response to selection due to measurement error can be derived from equation 5 by replacing the square root of heritability by the square root of the reduced heritability:

$$R_{ind}^{reduced} = i\sigma_A h_{reduced} = i\sigma_A \sqrt{\lambda}h = \sqrt{\lambda}R_{ind} \tag{9}$$

Two widely used methods in forest tree breeding is forward and backward selection. The most basic form of forward selection is selection of superior trees in the forest or in plantations (plus-trees) based upon the observed phenotype of individual trees without any information about genetic relationships (family structure). This implies the individual selection described above.

Backward selection is the process of selecting parent trees based upon breeding values estimated from progeny trials. Typically, the candidate parents are plus-trees from earlier selection in the forest. The response to backward selection is the difference in average trait value between a population generated from only the selected parents and a population generated from all candidate parents. The expected response to backward selection from open-pollinated plus-trees based upon a progeny trial is:

$$R_{bkw} = i \cdot \frac{\sigma_A}{\sqrt{1 + (4/h^2 - 1)/n}} \tag{10}$$

, where n is the number half-sibs from each mother in the trial (Ruotsalainen & Lindgren 1998). We assume here that the plus-tree population size is large and ignore corrections due to finite number of plus-trees. The only variable that changes when introducing a measurement error here is h^2 which decreases by the factor λ, and it follows that the response decreases with increasing measurement error, although in a more complicated way than is the case for individual selection:

$$R_{bkw}^{reduced} = \sqrt{\frac{h^2(n-1)/4 + 1}{h^2(n-1)/4 + 1/\lambda}} \cdot R_{bkw} = \sqrt{\kappa} \cdot R_{bkw} \tag{11}$$

, where $R_{bkw}^{reduced}$ is the reduced response in backward selection due to measurement error and $\kappa = \frac{h^2(n-1)/4 + 1}{h^2(n-1)/4 + 1/\lambda}$ is a reduction factor for backward selection analogous to λ for individual selection. It follows that:

$$\lambda \leq \kappa \leq 1 \tag{12}$$

This means that the relative reduction of the response to backward selection due to measurement error is less than or maximally the same as for individual selection, given the same h^2. The conditions for these relative reductions to be the same are that either $h^2 = 0$, the response is zero anyway, $\lambda = 1$, there is no random measurement error, or that $n = 1$, which would not be the case in practice.

We calculated the expected response to different selection intensities for these two selection regimes with and without estimated random measurement errors from the UAV measurements of height, using the estimated phenotypic variance (1.39 m^2) and mean (4.63 m) of height (H17) from the 241 manually measured trees in the trial.

Additionally, we calculated $\sqrt{\lambda}$ and $\sqrt{\kappa}$ for three genetic trials with Norway spruce trees for height in age 10 using the same estimated random measurement errors. These trials were complete diallels (Skrøppa et al. in prep.), so in fact both parents of the trees were known, but in order to calculate a representative $\sqrt{\kappa}$ we reanalyzed the trials as half-sibs, just using the random effect of mother to estimate the additive genetic variance. In addition, we fitted random effects of plot and replicate. The phenotypic variance was calculated as the sum of mother variance, plot variance and residual variance. The additive variance was calculated as four times the mother variance. Heritability was estimated according to equation 6. The number of half-sibs for each mother (n) was about 130, but for the sake the example we calculated $\sqrt{\kappa}$ for n = 4, 30 and 100. The average height was about 2 - 2.5 m for the different diallels.

Results

Tree height and total annual height growth

An overview of the models' performance is found in Table 2. For the sake of interpreting the sign of the mean error (ME) and the correlation between errors and actual trait value (r[(x-y),y]), note that these are calculated from the value of the predicted height (x) minus the actual height (y). The given percentages for the errors represent fractions of the phenotypic mean ($\bar{y}$) for the respective subset. All correlations between UAV measurements and manual measurements were significant (p<0.05). Except for the UAV variable CHMmx_6 all correlations between errors and manual measurements (validation data) were negative and significant (p<0.001). For the variable CHMmx_1 this relationship is illustrated in Figure 3B. Estimating individual tree height as the highest pixel value of the CHM within the tree's grid cell before start of the active growing period (CHMmx_1) yielded a total error (RMSE) of 0.93 m, a mean error (ME) of -0.45 m and a random error (SDE) of 0.82 m. The mean error indicates that tree heights were on average underestimated by 45 cm or 9.7% of the average height. Some trees were highly overestimated (Figure 2A).

Table 2. Statistics for estimation of total height accomplished by 2017, and total increment in 2018, from UAV derived variables (x) validated against manual measurements (y). The unit of the errors is meter.

y	x	N	RMSE	ME (x - y)	SDE	r[x,y] (p)[1]	r[(x-y),y] (p)[1]
H17	CHMmx_1	241	0.93 (20%)	-0.45 (-9.7%)	0.82 (18%)	0.73 (<0.001)	-0.77 (<0.001)
H17	CHMmx_1	131[2]	0.88 (17%)	-0.86 (-16%)	0.21 (4.0%)	0.96 (<0.001)	-0.36 (<0.001)
H17	CHMmx20_1	241	0.92 (20%)	-0.73 (-16%)	0.57 (12%)	0.88 (<0.001)	-0.67 (<0.001)
H17	CHMmx_6	241	0.80 (17%)	0.20 (4.3%)	0.78 (17%)	0.75 (<0.001)	-0.70 (<0.001)
H17	CHMmx_6	133[2]	0.19 (3.6%)	-0.12 (-2.3%)	0.14 (2.8%)	0.98 (<0.001)	0.07 (0.448)
H17	CHMmx20_6	241	0.62 (13%)	-0.13 (-2.9%)	0.61 (13%)	0.86 (<0.001)	-0.47 (<0.001)
G18	ΔCHMmx	241	0.44 (114%)	0.26 (69%)	0.35 (91%)	0.14 (0.029)	-0.37 (<0.001)
G18	ΔCHMmx	109[2]	0.35 (78%)	0.28 (62%)	0.21 (47%)	0.24 (0.014)	-0.41 (<0.001)
G18	ΔCHMmx20	241	0.44 (114%)	0.22 (57%)	0.38 (100%)	0.18 (0.005)	-0.29 (<0.001)

[1] Pearson's correlation coefficient between prediction and validation data (r[x,y]) and between errors and validation data (r[(x-y),y]) are shown with p value from a two-sided t-test.
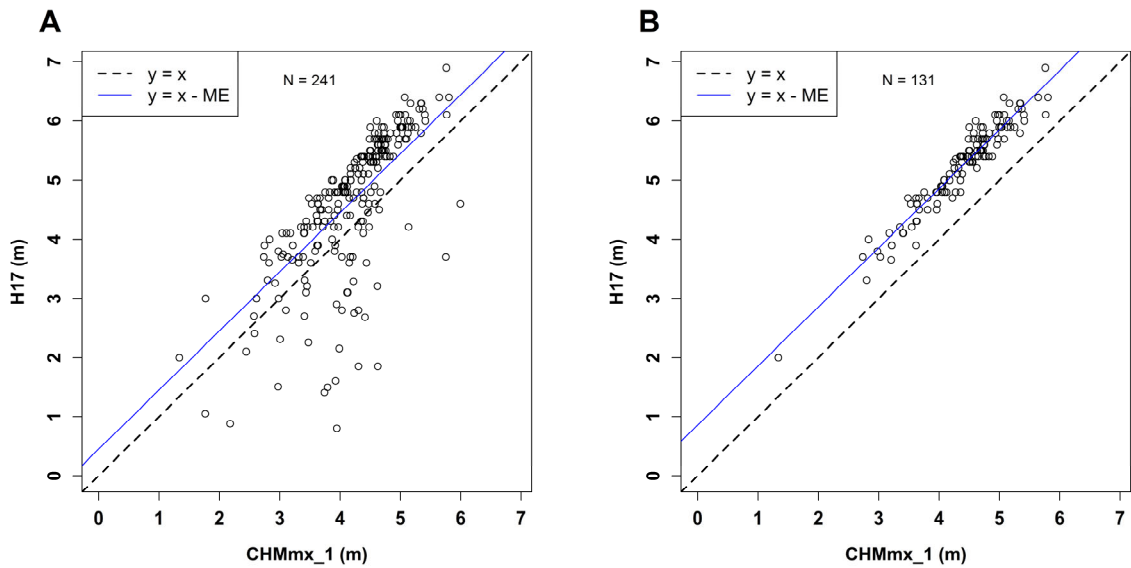
Figure2. Manual measurement of height 2017 fitted against the maximum grid cell value of the CHM from UAV measurements for all N=241 trees (A) and a subset (N=131) where the highest estimated point within the grid cell (assumed to be a tree top) was at least 25 cm from each cell edge (B).

The most overestimated trees were those where the highest estimated point within the grid cell, assumed tree top, was located close to the nearest grid cell edge (Figure 3A). These were mainly the smaller trees (Figure 3B). Examples can be found in Figure 4.
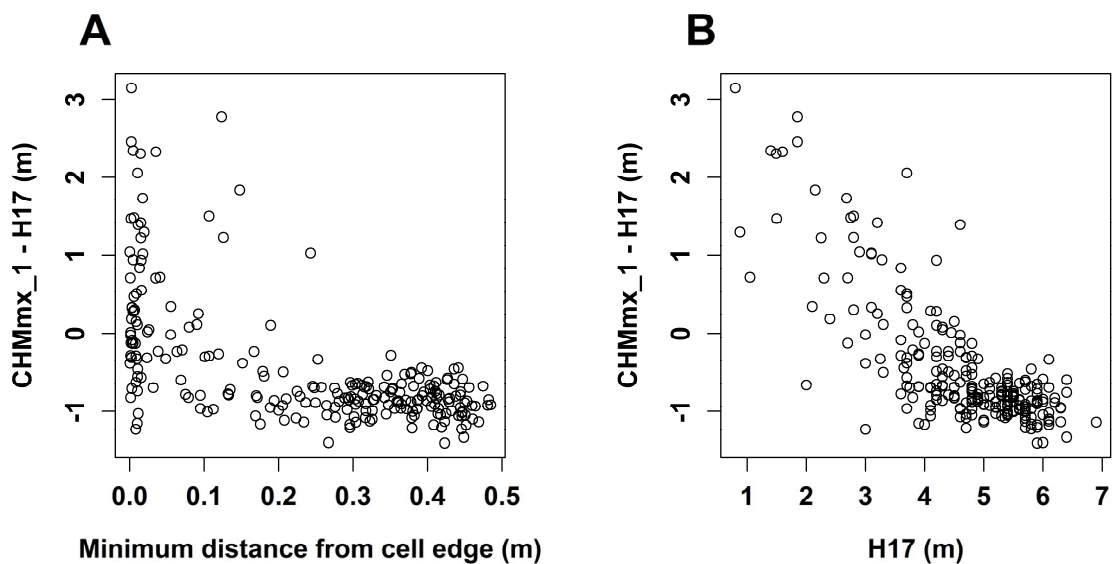

Figure 3. The errors of the UAV-based measurements plotted against the distance of the point of CHMmx from nearest grid cell edge (A) and against tree height (B).

The highest estimated point within a 20 cm radius from the grid cell center (CHMmx20_1) showed lower random error (SDE) and more negative mean error (ME) than CHMmx_1 (Table 2). For CHMmx_1 with a reduced data set (N=131) omitting trees where the point of CHMmx_1 was closer than 25 cm to the nearest cell edge, we obtained a lower total error (RMSE) a lower random error (SDE), a higher correlation between predicted values and validation data and a less negative correlation between errors and validation data. However, the mean error (ME) became more negative (Table 2). This is illustrated in Figure 2B.

The explanatory variable CHMmx_6 yielded a positive ME of 0.20 m, i.e. a mean overestimation of 4% when the whole dataset (N=241) was used. For the reduced dataset (N=133), where trees where the point of CHMmx_6 was closer than 25 cm from the cell edge were removed, the mean error was -0.12 m, i.e. a mean underestimation of 2.3%. This variable showed the lowest RMSE and SDE and the highest correlation between UAV measurements and manual measurements of total tree height accomplished by 2017. It was also the only variable without a significant correlation between errors and actual trait values. The variable CHMmx20_6 showed a ME of -0.13 m and a less negative correlation between errors and actual trait values than the other variables when using the whole dataset (Table 2).

Examples illustrating some of the problems with both CHMmx and CHMmx20 are found in Figure 4.
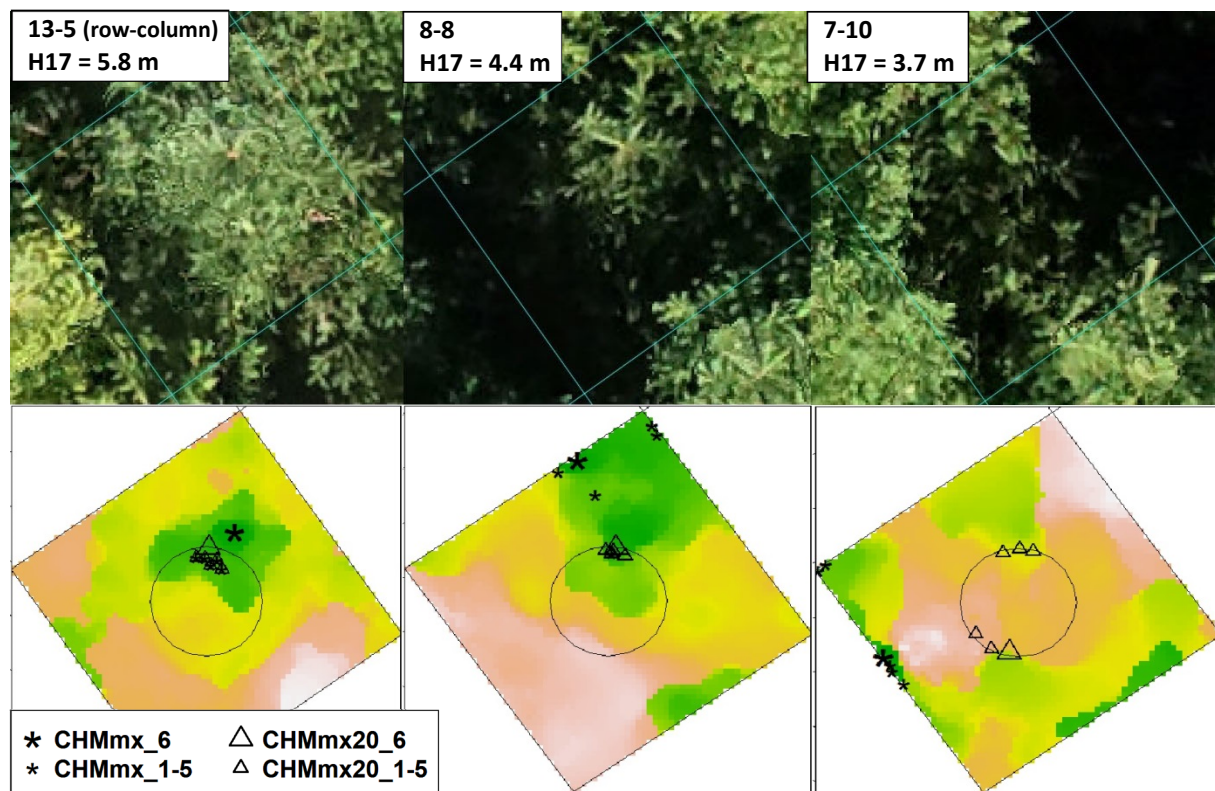

Figure 4. Orthophotos (top) and CHM (bottom) of three grid cells on the last date of UAV measurement (October 18, 2018). The circle indicates the 20 cm radius used for the CHMmx20 variables.

The estimates of height increment in 2018 (G18), the difference CHMmx_6 - CHMmx_1 or CHMmx20_6 - CHMmx20_1, showed positive MEs ranging 0.22-0.28 m, i.e. relative overestimations of 57-69%. The SDEs ranged 0.21-0.38 m (47-100%). They all showed very weak (r<0.24) but still significant (p<0.05) correlations with manually measured values.

The evaluation of the DTM by the 49 height reference points showed that the average difference between the measured elevation and the DTM elevation (the former minus the latter) was -10 cm. This implies that the DTM overestimates ground elevations in the trial by 10 cm. The only obvious spatial tendency was that points on the south-western edge of the trial tended to be more overestimated. Only one of the 49 points was underestimated. The RMSE was 0.124 m and the standard deviation was 0.075 m. The range was -0.230 to +0.193 m.

Phenology

For the fitting of growth curves 850 trees had a manually scored Krutzsch value for bud flush and a complete set of values for CHMmx on all six dates. Out of the 850 trees we were able to fit curves for 702. By visual inspection (of 100 randomly selected trees) many of the trees had been assigned values which were not realistic due to e.g. a very large extrapolation, or unreasonable values of some points (such as values < 0 or > 1). Examples of curves can be seen in Figure 5.

Correlations between UAV-derived phenology variables and manually scored Krutzsch were generally weak (Table 3). For the full dataset, significant negative correlations were only found between Day05 estimate from CHMmx20 and Krutzsch score. The same was observed when growth curves were based upon CHMmx for trees where the distance of the points of both CHMmx_1 and CHMmx_6 from the nearest grid cell edge were at least 25 cm.

Table 3. Pearson's correlation coefficient (r) between normal score transformed Krutzsch score and Day05 and Day95 with p-value from t-test. Where sample size (N) is marked with an asterisk (*) the only trees included were those whose points of CHMmx_1 and CHMmx_6 were both at least 25 cm from the nearest grid cell edge.

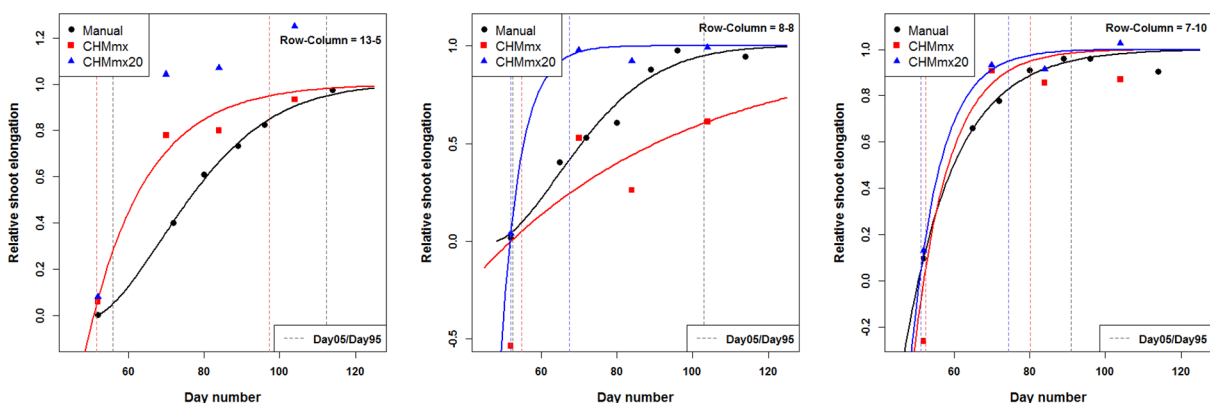| UAV-derived phenology variable	UAV-variable	N	r (p)
Day05	CHMmx	702	-0.05 (0.233)
Day95	CHMmx	702	0.06 (0.119)
Day05	CHMmx	397*	-0.27 (<0.001)
Day95	CHMmx	397*	0.03 (0.548)
Day05	CHMmx20	646	-0.19 (<0.001)
Day95	CHMmx20	646	0.02 (0.607)

Figure 5. Estimated growth curves for three trees based upon measures from photographs of tree tops (Manual) and based upon the UAV variables CHMmx and CHMmx20. The position of the trees in the trial as

row-column were 13-5, 8-8, 7-10 from left to right on the figure. Day numbers refer to number of days from 1st of April. The Weibull curve could not be fitted for the CHMmx20 variable for tree 13-5.

Implications for breeding

The predicted response to selection is differently affected depending on whether the selection is forward or backward, and whether the backward selection is based on 4, 30 or 100 individuals per family (Table 4). An SDE of 0.78 m reduces the response to forward selection to 43-83 % ($\sqrt{\lambda}$) of the full response (SDE=0), while an SDE of 0.14 only reduces the response to 93-99 %. In backward selection, the larger error of 0.78 m is more critical in small family sizes (n=4) as the response is reduced to 46-85 % ($\sqrt{\kappa}$), compared to large family sizes (n=100) where the response is 80-93 % compared to the case with SDE = 0. An SDE of 0.14 m has no practical implications in backward selection regardless of family size. The response curves over selection intensities for the UAV trial, shown in Figure 6, indicate that the loss in response might be marginal in trials were phenotypic variation is large. The corresponding reduction factors for the response to individual selection ($\sqrt{\lambda}$) and backward selection ($\sqrt{\kappa}$) are given in the figure legends.
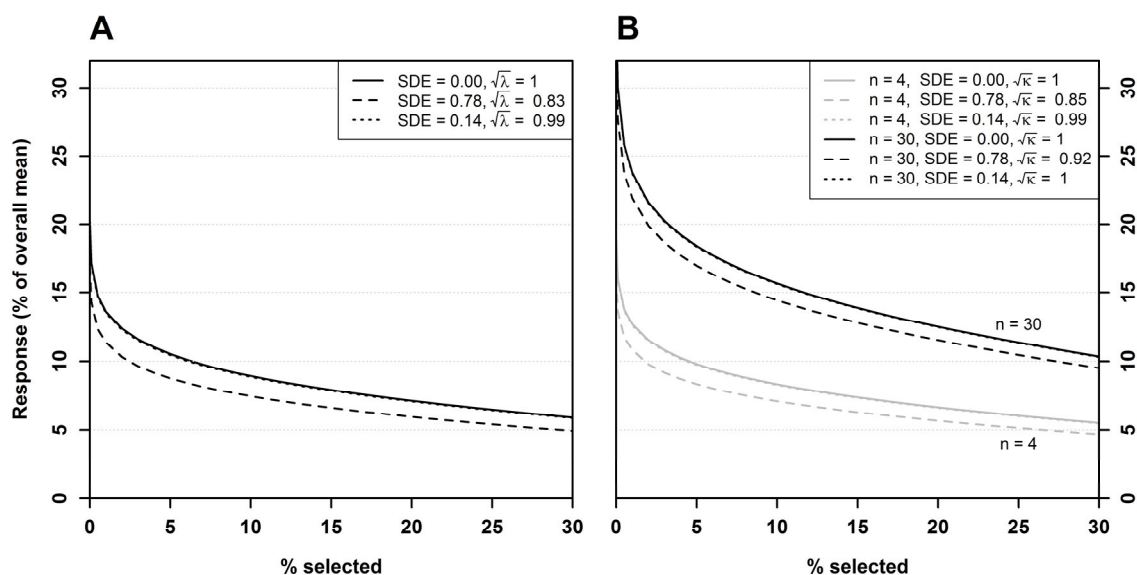

Figure 6. The expected response to selection for typical measurement errors (SDE) given a h² = 0.20, V_p = 1.39 and $\overline{y}$ = 4.63 for individual forward selection (A) and backward selection (B) with family size n. The effect of SDE=0.14 is so small that the response is virtually indistinguishable from the response when SDE=0.

Table 4. The effect of random measurement error on the response to individual and backward selection expressed as the proportions $\sqrt{\lambda}$ and $\sqrt{\kappa}$, respectively (cf. equations 9 and 11), for variance estimated from different trials. The parameter n is the hypothetical family size in a balanced progeny trial. The diallels used for parameter estimation are described in Skrøppa et al. (in prep.).

Trial	h²	V_p	SDE	$\sqrt{\lambda}$		n	$\sqrt{\kappa}$
Diallel 1	0.276	0.135	0.78	0.43		4/30/100	0.46/0.63/0.80
			0.14	0.93		4/30/100	0.94/0.98/0.99
Diallel 2	0.201	0.193	0.78	0.49		4/30/100	0.52/0.66/0.81

			0.14	0.95		4/30/100	0.96/0.98/0.99
Diallel 3	0.185	0.195	0.78	0.49		4/30/100	0.52/0.65/0.80
			0.14	0.95		4/30/100	0.96/0.98/0.99
UAV trial	0.2 (hypothetical)	1.39	0.78	0.83		4/30/100	0.85/0.92/0.97
			0.14	0.99		4/30/100	0.99/1.00/1.00

Discussion

Tree height and total annual height increment

The evaluation of measurement accuracy for total tree height (H17) was done progressively as the obvious sources of error were identified. The main statistics for this evaluation were the mean error (ME) which exposes the bias (over or under estimate), the random error (SDE) which can be considered as the pure measurement error if the bias is ignored, and the total measurement error (RMSE). Estimates of tree height were performed on basis of the CHM from the first and last flight in 2018. Intuitively, the first flight should represent total tree heights accomplished at the end of the growing season of 2017 (H17), and the last flight should represent the final height accomplished after 2018.

At first glance, the UAV measurements yielded a RMSE of 93 cm, or 20 % of mean tree height, when the highest pixel within each grid cell from the flight (CHMmx_1) was used as estimate of H17 (Table 2). While some trees were underestimated, most smaller trees were highly overestimated (Figure 2A). We identified that the location of the pixel with the highest value (CHMmx) for these trees was from a position close to the boundary of the expected grid cell of the target tree. It therefore seems likely that these values do not represent the very apex of the target tree, but rather a branch from a taller neighboring tree. This *misidentification* is exemplified in Figure 4, with three different cases. For both the cases 8-8 and 7-10 the point of CHMmx is situated close to the cell edge and probably represents a side-branch from a neighboring tree. The use of variable CHMmx20 is possibly resolving this issue in the case 8-8 but not in the case 7-10. In the case 13-5 the variable CHMmx20 seems to miss the tree top on the last date. It is not necessarily easy to locate the tree top from visual inspection of the orthophotos either, as illustrated in the case 7-10.

The misidentification of the tree tops might be avoided if a better method of determining the position of the crowns were used. One possibility could be to position the trees by GPS when they were planted or combining automatic detection with visual inspection of the orthomosaic and CHM as did Krause et al. (2019). A more automated solution could perhaps be to use advanced machine-learning image recognition of tree crowns such as those used by Weinstein et al. (2019). This might have reduced the errors we obtained. On the other hand, we assumed that information of dead/missing trees was available, as such trees have not been included in the analyses. If this information were not available, and all detection of missing trees were to be performed by image analysis, the error could increase.

We partly resolved the problem by either using the local maximum within a 20 cm radius of the grid cell center (CHMmx20) or by excluding trees where the location of CHMmx_1 was closer than 25 cm from the nearest grid cell edge (CHMmx_1 with N=131 in Table 2). This resulted in an SDE of only 21 cm (4 %), but negative ME from 0.73 to 0.86, i.e. a strong underestimation suggesting that CHM is

not capturing the very apex of the leader. This is reasonable as the resolution of the CHM of approximately 2 cm x 2 cm is larger than the cross section of the apical bud. Furthermore, it is rather typical for photogrammetric data to create somewhat smooth 3D surfaces and this may further explain the systematic under-estimation of tree heights. Measuring tree heights of Scots pine with similar UAV methods Krause et al. (2019) obtained a mean error of only -13 cm although they used a rougher resolution and the trees were taller. Estimating heights of *Pinus pinea* Guerra-Hernández et al. (2017) also suggested that smoothing in the image processing caused a slight underestimation.

The effect was confirmed as average underestimation was much less severe (-12 to +20 cm) when H17 was estimated from the last UAV flight in 2018 (CHMmx_6 and CHMmx20_6). Then the annual height elongation had ceased and a new whorl was formed at the apex of the 2017-shoot. The random error did not change much, except that it was reduced to 14 cm for trees where CHMmx was minimum 25 cm away from the grid cell edge. Our validation data, however, also contain measurement errors from the manual measurements with the rod. It is not unlikely that this is a random error in the range 5 – 10 cm.

Furthermore, the validation of the ground elevation data revealed that the digital terrain model (DTM) overestimated the ground elevation by 10 cm on average. This translates directly into a 10 cm average underestimation of the CHM, which explains the remaining ME. If the absolute heights of the trees are important, such errors in the DTM should be taken into account. For the random part of the measurement error, however, the DTM error is not critical for the type of ground conditions represented by this trial. In the forest, however, local variations in ground elevation could be much higher, augmenting the need for high-resolution DTMs. It is worth noting that even the height reference points used for validation of the DTM could contain errors due to the dense forested environment, but these were the best height estimates we were able to obtain.

Because the apex was not represented properly by the CHM, it is not surprising that estimates of height increments had high relative errors. Still, there were significant correlations between the UAV estimates and the manual measurements. It might be that the UAV variables approximated the growth from the year before as the height difference between the uppermost whorl before and after the 2018 season. That growth is likely to correlate with the growth in 2018.

Phenology

When the highest pixel value of the CHM within each grid cell (CHMmx) at each date of UAV-flight was used to estimate growth curves and calculate a proxy for growth start (Day05) the correlation with bud flush (Krutzsch score) was low and not statistically significant when the whole dataset was included. Since the CHM seems unable to detect the apex of the leader shoot it is likely that the growth curves are not representing the growth of the leader shoot. They might still, however, reflect the growth period of the tree as a new whorl is forming over the course of the growth period making the local maximum of the CHM increase over time, but not necessarily with a curve like the growth curve of the leader.

When using the highest pixel value of the CHM within a 20 cm radius of the grid cell center (CHMmx20) instead, a significant correlation was found. A major problem with the CHM was the inability to always correctly identify the target tree for instance due to branches of taller neighbors. Some examples are shown in Figure 4. A significant correlation was also found using CHMmx if we excluded trees where the location of CHMmx was closed than 25 cm from the nearest grid cell edge.

These correlations were weak, however, and the method does not seem accurate enough for efficient characterization of the phenology of apical meristems on an individual tree level. Other methods might be more effective. Berra et al. (2019) also looked at timing of vegetative phenology events on an individual tree level using data obtained with UAV-techniques. They used Green Chromatic Coordinate (GCC) and Normalized Difference Vegetation Index (NDVI) to estimate start, middle and end of spring season. They obtained an R^2 as high as 0.82 and a RMSE as low as 8 days for start of spring season using GCC when analyzing individual trees of different species of deciduous and evergreen trees together. However, the uncertainties seemed higher for the evergreen species, including Norway spruce.

Implications for breeding

The component of the measurement error relevant for breeding is the random error (SDE). Assuming this error is independent of the actual trait value we have presented the expected relative reduction in genetic gain (response to selection) for two commonly used selective regimes, individual forward selection (e.g. selection of plus-trees in a forest plantation) and backward selection of parents based upon progeny trials (equations 9 and 11 respectively). The derivation of equations 9 and 11 shows that the relative reduction in response to selection due to the random measurement error (SDE) depends only on the variance of the measurement error and the phenotypic variance in the case of individual selection, whereas it also depends on family size and the heritability in the case of backward selection.

The assumption that the random error (SDE) is independent of actual trait value is clearly violated in the case of the full dataset, since the lowest trees are systematically overestimated (Figures 2-3). Most of the UAV-variables for total height have errors correlated negatively with actual trait value (Table 2), indicating an overestimation of the lower trees (and underestimation of tall trees). Only the variable CHMmx_6 on the subset (N=133) may possibly have a random error completely independent of actual trait value, as the correlation between error and trait here is insignificant.

We also calculated these measures for three genetic trials (diallels) (Skrøppa et al. in prep.) reanalyzed as progeny trials with half-sibs (Table 4). The negative effects of measurement error were more severe in these trials due to the lower phenotypic variance. This is based upon the assumptions that the measurement error would be the same in those trials although the mean tree heights were considerably lower than in the UAV trial. Nevertheless, for the lowest measurement error (SDE=14 cm) $\sqrt{\lambda}$ ranged from 0.93 to 0.95 and $\sqrt{\kappa}$ ranged from 0.94 to 0.99 in the diallel trials even with a family size (n) as low as 4. In practical tree breeding, the two selection scenarios are different in respect to what is the critical measurement error. In individual forward selection, only the largest trees are of interest and there is no need to phenotype intermediate and small individuals. Hence, it is relevant to evaluate the method in terms of the reduced dataset, focusing only on the large trees most likely correctly identified (N=133). The measurement error (SDE) of these trees was 0.14 cm, which yield a response from 93 to 95 % of the full response expected from manual measurements in the three diallels used as examples (Table 4).

In backward selection of the best parents after progeny test, however, the breeder is more dependent on phenotyping also intermediate and suppressed trees to obtain the full family variance for breeding value estimation. The breeder must then expect a measurement error (SDE) of 0.78 m and a reduced heritability. If the breeder has only one site available, with typical 30 trees per family,

the gain obtained would come to about 65 % of the gain expected from manual measurements. A larger trial, or a set of several trials, would make the family size larger and the relative response higher (Table 4). However, in this case the assumption of a random distributed error is violated since the smaller trees are highly overestimated. The problem of misidentification must be solved, possibly with an earlier measurement before canopy closure to position the trees in the grid and identify missing trees.

For both selection scenarios, it is evident that the measurement error affects the response to selection. However, as the number of phenotyped trees and family size most often are limited by the budget, more effective methods for phenotyping could potentially increase the size of the trials and materials phenotyped. Hence, the genetic base for selection could be expanded and the genetic gain increased.

Although the UAV-method was inappropriate for the estimation of intra-annual growth curves, we found a weak correlation between Day05 (UAV-derived) and Krutzsch score (manual score). It may therefore be possible that the UAV-derived growth start proxy could be used to rank varieties on an aggregated level, such as family or provenance. As the trial did have a structure with combinations between different genotypes and temperature treatments known to have caused differences in phenology (Kvaalen & Johnsen 2008) we calculated the correlation between Day05 and Krutzsch for the mean values across these combinations (data not shown). We did not find significant correlations, however.

It has been predicted that phenotyping based upon remote sensing could improve gain by increasing the number of individuals to select among and therefore the selection intensity (Dungey et al. 2018; Lstibůrek et al. 2017). This could be done by selection of superior individuals in large plantations in combination with molecular genotyping techniques or possibly prior knowledge of genetic relationships to replace the time-consuming and expensive traditional genetic trials, such as in Breeding Without Breeding (El-Kassaby & Lstiburek 2009; Lstibůrek et al. 2017). If ground elevations are also more variable in the forest, there may be need for a higher resolution DTM than the one we have used here. More variable ground elevations should translate into an increased random measurement error and therefore reduce the response according to the equations we have used here for the given selection regimes. On the other hand, the canopy in the forest would rarely be as densely closed as in this trial. Therefore, an ALS-based DTM could be more accurate, and identification of tree tops could be easier. If tree positions are properly identified our results indicate that UAV measurements should be sufficiently accurate for selection for increased height growth.

Transferability of the method
The method of height measurement presented here is relatively simple and intuitive because it uses local maxima from a DSM to represent tree tops. The DSM is generated with well-established photogrammetric methods, and by simply subtracting the DTM from the DSM a CHM is established. We intentionally avoided fitting a model to the manual measurements. Fitting a simple regression model or combining different variables obtainable from processing the RGB images might have shown lower errors in the present trial, but using such a model in different trials would require extensive validation because the specific variable combinations and model coefficients would not have an intuitive interpretation, and could be different had the model been fitted in a different trial. Understanding what causes such differences could be difficult, whereas the technique presented

here represents a measurement method rather than a statistical model and should therefore be easily transferable to other trials. Moreover, with this simple, intuitive approach we were able to find plausible reasons why some trees were highly overestimated and suggest ways avoid the problem. For the same reasons we wanted to test the possibility to estimate phenology traits by using heights measured with UAV and fit a growth curve to these measurements in the same way as one could do with manual measurements. However, this attempt was rather unsuccessful due to the difficulty of representing the apex of the leader in the CHM.

Conclusions

The precision of total tree height measurements of Norway spruce in a dense field trial using UAV is adequate for efficient breeding. This is under the condition that only the tallest trees are to be phenotyped (forward selection) or that side branches from taller neighbors are not misidentified as tree tops of suppressed trees. The observed mean error indicates that the measured height is approximately the height of the uppermost whorl and thus last year's height rather than current year. This creates problems when trying to represent the intra-annual growth and phenology of the trees.

Acknowledgements

Literature

Agisoft. (2019). *Agisoft Metashape User Manual*. Professional Edition, Version 1.5 ed.: Agisoft LLC. Available at: https://www.agisoft.com/pdf/metashape-pro_1_5_en.pdf.

Axelsson, P. (2000). DEM generation from laser scanner data using adaptive TIN models. *The International Archives of the Photogrammetry, Remote Sensing and Spatial Information Sciences*, 33: 110-117.

Berra, E. F., Gaulton, R. & Barr, S. (2019). Assessing spring phenology of a temperate woodland: A multiscale comparison of ground, unmanned aerial vehicle and Landsat satellite observations. *Remote Sensing of Environment*, 223: 229-242.

Blom. (2014). *LiDAR-rapport*. Available at: https://hoydedata.no/LaserInnsyn/ProsjektRapport?filePath=%5C%5Cstatkart.no%5Choydedata_orig%5Cvol1%5C119%5Cmetadata%5CFollo%202014_Prosjektrapport.pdf.

Blom, G. (1958). *Statistical estimates and transformed beta-variables*. Stockholm: Almqvist & Wiksell.

Dempewolf, J., Nagol, J., Hein, S., Thiel, C. & Zimmermann, R. (2017). Measurement of within-season tree height growth in a mixed forest stand using UAV imagery. *Forests*, 8 (7): 15.

DJI. (2016). *Phantom 4 PRO/PRO+ user manual*. Available at: https://dl.djicdn.com/downloads/phantom_4_pro/Phantom+4+Pro+Pro+Plus+User+Manual+v1.0.pdf.

DJI. (2018). *DJI GS PRO user manual*. Available at: https://dl.djicdn.com/downloads/groundstation_pro/20181102/GS_Pro_User_Manual_v2.0_EN_201811.pdf.

Dungey, H. S., Dash, J. P., Pont, D., Clinton, P. W., Watt, M. S. & Telfer, E. J. (2018). Phenotyping whole forests will help to track genetic performance. *Trends in Plant Science*, 23 (10): 854-864.

El-Kassaby, Y. A. & Lstiburek, M. (2009). Breeding without breeding. *Genetics Research*, 91 (2): 111-120.

Falconer, D. S. & Mackay, T. F. C. (1996). *Introduction to Quantitative Genetics*. 4th ed. ed. Harlow, England: Pearson.

Ganz, S., Käber, Y. & Adler, P. (2019). Measuring tree height with remote sensing—A comparison of photogrammetric and LiDAR data with different field measurements. *Forests*, 10 (8): 14.

Guerra-Hernández, J., González-Ferreiro, E., Monleón, V. J., Faias, S. P., Tomé, M. & Díaz-Varela, R. A. (2017). Use of multi-temporal UAV-derived imagery for estimating individual tree growth in Pinus pinea stands. *Forests*, 8 (8): 19.

Haapanen, M., Jansson, G., Nielsen, U. B., Steffenrem, A. & Stener, L.-G. (2015). The status of tree breeding and its potential for improving biomass production - A review of breeding activities and genetic gains in Scandinavia and Finland. In Stener, L.-G. (ed.). Uppsala: Skogforsk.

Jansson, G., Hansen, J. K., Haapanen, M., Kvaalen, H. & Steffenrem, A. (2017). The genetic and economic gains from forest tree breeding programmes in Scandinavia and Finland. *Scandinavian Journal of Forest Research*, 32 (4): 273-286.

Karpina, M., Jarząbek-Rychard, M., Tymków, P. & Borkowski, A. (2016). *UAV-based automatic tree growth measurement for biomass estimation*. ISPRS The International Archives of the Photogrammetry, Remote Sensing and Spatial Information Sciences, Prague, Czech Republic, pp. 685-688: The International Archives of the Photogrammetry, Remote Sensing and Spatial Information Sciences.

Klosterman, S. & Richardson, A. D. (2017). Observing spring and fall phenology in a deciduous forest with aerial drone imagery. *Sensors*, 17 (12): 17.

Krause, S., Sanders, T. G. M., Mund, J.-P. & Greve, K. (2019). UAV-based photogrammetric tree height measurement for intensive forest monitoring. *Remote Sensing*, 11 (7): 18.

Krutzsch, P. (1973). *Norway spruce development of buds*. IUFRO S2.02.11. Stockholm: The Royal College of Forestry.

Kvaalen, H. & Johnsen, Ø. (2008). Timing of bud set in Picea abies is regulated by a memory of temperature during zygotic and somatic embryogenesis. *New Phytologist*, 177 (1): 49-59.

Larjavaara, M. & Muller-Landau, H. C. (2013). Measuring tree height: a quantitative comparison of two common field methods in a moist tropical forest. *Methods in Ecology and Evolution*, 4 (9): 793-801.

Lstibůrek, M., El-Kassaby, Y. A., Skrøppa, T., Hodge, G. R., Sønstebø, J. H. & Steffenrem, A. (2017). Dynamic gene-resource landscape management of Norway spruce: Combining utilization and conservation. *Frontiers in Plant Science*, 8: 6.

Park, J. Y., Muller-Landau, H. C., Lichstein, J. W., Rifai, S. W., Dandois, J. P. & Bohlman, S. A. (2019). Quantifying leaf phenology of individual trees and species in a tropical forest using unmanned aerial vehicle (UAV) images. *Remote Sensing*, 11 (13): 32.

Ponzi, E., Keller, L. F., Bonnet, T. & Muff, S. (2018). Heritability, selection, and the response to selection in the presence of phenotypic measurement error: Effects, cures, and the role of repeated measurements. *Evolution*, 72 (10): 1992-2004.

Puliti, S., Solberg, S. & Granhus, A. (2019). Use of UAV photogrammetric data for estimation of biophysical properties in forest stands under regeneration. *Remote Sensing*, 11 (3): 15.

R Core Team. (2017). *R: A language and environment for statistical computing*. Vienna, Austria: R Foundation for Statistical Computing.https://www.R-project.org/

Rasband, W. S. (1997-2008). *ImageJ*. Bethesda, Maryland, USA: U. S. National Institutes of Health.https://imagej.nih.gov/ij/

Ruotsalainen, S. & Lindgren, D. (1998). Predicting genetic gain of backward and forward selection in forest tree breeding. *Silvae Genetica*, 47 (1): 42-50.

Santini, F., Kefauver, S. C., de Dios, V. R., Araus, J. L. & Voltas, J. (2019). Using unmanned aerial vehicle-based multispectral, RGB and thermal imagery for phenotyping of forest genetic trials: A case study in Pinus halepensis. *Annals of Applied Biology*, 174 (2): 262-276.

Skrøppa, T., Solvin, T. M. & Steffenrem, A. (in prep.). Diallel crosses in Picea abies. III. Variation and inheritance patterns in nursery and short-term trials.

Topcon. (2018). *Gr-5 Advanced Gnss Receiver*. Available at: https://www.topcon.co.jp/en/positioning/products/pdf/GR-5_E.pdf.

Torres-Sánchez, J., López-Granados, F., Serrano, N., Arquero, O. & Peña, J. M. (2015). High-throughput 3-D monitoring of agricultural-tree plantations with unmanned aerial vehicle (UAV) technology. *Plos One*, 10 (6): 20.

Weinstein, B. G., Marconi, S., Bohlman, S., Zare, A. & White, E. (2019). Individual tree-crown detection in RGB imagery using semi-supervised deep learning neural networks. *Remote Sensing*, 11 (11): 13.